

Improved fits of the effective masses at Γ in the spin-orbit, second-nearest-neighbor sp^3s^* model: Results from analytic expressions

Timothy B. Boykin

Department of Electrical and Computer Engineering, University of Alabama in Huntsville, Huntsville, Alabama 35899

(Received 18 April 1997)

We derive and study exact analytic expressions for the effective masses of the conduction—and *all three* hole—bands at Γ in the spin-orbit, second-nearest-neighbor sp^3s^* model. Using these expressions we determine parameters for six common III-V materials (GaAs, AlAs, GaSb, AlSb, InAs, and InP), tailored for [001]-oriented heterostructure calculations. Beyond their use in fitting band structures, the effective-mass formulas show that the second-nearest-neighbor sp^3s^* model is not without limitations. We show that there is an upper bound on the reproducible electron–light-hole effective-mass mismatch, so that even this model may not be sufficient for certain materials. [S0163-1829(97)01339-8]

Empirical tight-binding techniques are becoming increasingly common in semiconductor heterostructure calculations, such as those for resonant tunneling diodes (RTD's), quantum wells (QW's), and superlattices (SL's). Although it would seem obvious that the successful use of such approaches requires carefully choosing the parameters so that the relevant effective masses and energy gaps are properly reproduced, this is all too often not the case. That is, most parametrizations seek to achieve a *global* fit, rather than concentrating on those band-structure features of greatest importance for heterostructure modeling. Furthermore, because the few possible analytic solutions for these models remain largely unexplored, most workers tend to ascribe too much flexibility to them. As a result, many heterostructure calculations have been based upon insufficiently complete or poorly parametrized tight-binding models.

A careful analysis of those closed-form results that are obtainable resolves both of these problems. Most obviously, analytic formulas are of great aid in fitting parameter sets. More importantly and more subtly, when faced with a parameter set that does not fit certain band-structure features, they alone can determine whether the failure arises from limitations of the underlying model or merely from not having found the best parametrization. As an example, consider tight-binding models for semiconductor heterostructure calculations in [001]-oriented devices in which non- Γ -valley transport is expected to be important; for these devices we need a model that can correctly fit the X valleys. Examining first the computationally convenient nearest-neighbor sp^3s^* model¹ we see that it is inadequate: its characteristic polynomial along $(k_x, 0, 2\pi/a)$ is independent of k_x so that it cannot fit the X -valley transverse mass.² On the other hand, trial and error shows that including second-nearest-neighbor interactions with either the sp^3 (Ref. 3) or sp^3s^* (Ref. 4) basis set (the latter generally gives a better fit of the conduction bands) eliminates this difficulty. Hence, second-nearest-neighbor models merit further study.

Such an investigation is needed because to date there has been no thorough study of the capabilities and limitations of second-nearest-neighbor approaches, doubtless due to their complexity. Very recently Loehr and Talwar⁵ have found

analytic expressions for the electron and heavy-hole masses in the no-spin-orbit second-nearest-neighbor sp^3 model, but their results do not go far enough. First, a spin-orbit model is absolutely essential for modeling valence-band or interband heterostructures. Furthermore, our earlier work on nearest-neighbor models⁶ shows that including the spin-orbit interaction can benefit conduction-band heterostructure calculations as well. As we demonstrate in Ref. 6, including the spin-orbit interaction is generally necessary to properly fit the light-hole mass, thereby ensuring the correct imaginary-band dispersion (and hence attenuation) in barrier materials. (Reference 5 does *not* give the light-hole mass in the no-spin-orbit model.) Second, Loehr and Talwar⁵ do not attempt to fit either of the X -valley masses. Thus, spin-orbit parametrizations that better fit the X -valley masses along with analytic expressions for the masses at Γ are needed. Although Ref. 5 suggests that the latter are difficult to obtain we have found them using methods like those we employed earlier.⁶ Here we derive and study the analytic expressions for the (inverse) effective masses of electrons, heavy, light, and split-off holes at Γ in the second-nearest-neighbor, spin-orbit sp^3s^* model. Using these expressions, we determine parameters for six common semiconductor materials (GaAs, AlAs, GaSb, AlSb, InAs, and InP), tailored for use in [001]-oriented heterostructure calculations. Finally, from these expressions we show that, surprisingly, there is an upper limit on the electron–light-hole effective-mass mismatch $|m_{lh}^*/m_e^*|$ achievable with the second-nearest-neighbor sp^3s^* model.

We consider the second-nearest-neighbor sp^3s^* Hamiltonian in which both the nearest- and second-nearest-neighbor s - s^* and s^* - s^* interactions are set to zero. At $\mathbf{k} = \mathbf{0}$ both this matrix and the nearest-neighbor version take the same form, so that we may continue to employ the generic notation introduced in Ref. 6. The parameters for the various materials in the Slater-Koster⁷ notation, along with our abbreviations for those appearing in the effective-mass expressions, are given in Table I. The band energies and eigenvectors at $\mathbf{k} = \mathbf{0}$ are found by substituting the appropriate quantities from Table II into the generic equations below:

TABLE I. Tight-binding parameters (in eV) using the notation of Ref. 7 along with our abbreviations for those appearing in the text.

Abbrev.	Parameter	GaAs	AlAs	GaSb	AlSb	InAs	InP
E_{sa}	$E_{sa,sa}^{(000)}$	-8.487 06	-8.203 43	-4.974 14	-8.374 17	-9.581 10	-6.845 92
E_{pa}	$E_{pa,pa}^{(000)}$	0.387 69	-0.341 76	0.591 30	0.043 62	0.208 90	0.369 13
E_{s^*a}	$E_{s^*a,s^*a}^{(000)}$	8.487 69	6.512 48	8.150 00	7.401 56	7.409 90	9.730 00
E_{sc}	$E_{sc,sc}^{(000)}$	-2.861 11	-2.480 93	-2.604 92	-2.709 80	-2.497 90	-1.963 28
E_{pc}	$E_{pc,pc}^{(000)}$	3.567 69	2.119 99	3.240 86	2.991 51	3.306 10	3.012 56
E_{s^*c}	$E_{s^*c,s^*c}^{(000)}$	6.617 69	5.035 93	6.666 75	7.000 00	6.740 10	9.000 00
$V_{s,s}$	$4E_{sa,sc}^{(\frac{1}{2}\frac{1}{2}\frac{1}{2})}$	-6.460 53	-7.160 00	-4.820 00	-7.177 80	-5.381 30	-5.187 33
$V_{sa,pc}$	$4E_{sa,pc}^{(\frac{1}{2}\frac{1}{2}\frac{1}{2})}$	4.680 00	5.072 00	3.808 36	5.774 08	3.035 40	3.879 41
$V_{s^*a,pc}$	$4E_{s^*a,pc}^{(\frac{1}{2}\frac{1}{2}\frac{1}{2})}$	4.650 00	3.280 00	4.757 93	4.930 00	2.498 40	3.780 29
$V_{pa,sc}$	$4E_{pa,sc}^{(\frac{1}{2}\frac{1}{2}\frac{1}{2})}$	8.000 00	8.000 00	6.978 62	8.377 80	6.338 90	6.349 33
V_{pa,s^*c}	$4E_{pa,s^*c}^{(\frac{1}{2}\frac{1}{2}\frac{1}{2})}$	6.000 00	1.750 00	5.366 84	4.308 50	3.909 70	2.017 04
$V_{x,x}$	$4E_{x,x}^{(\frac{1}{2}\frac{1}{2}\frac{1}{2})}$	2.260 95	1.940 00	1.893 76	2.058 57	1.839 80	1.908 14
$V_{x,y}$	$4E_{x,y}^{(\frac{1}{2}\frac{1}{2}\frac{1}{2})}$	5.170 00	4.500 00	4.610 63	5.042 64	4.469 30	4.400 00
$V_{sa,sa}$	$4E_{sa,sa}^{(110)}$	-0.010 00	-0.010 00	-0.018 60	-0.010 00	-0.009 00	-0.009 30
$V_{sa,xa}$	$4E_{sa,xa}^{(110)}$	0.050 00	0.040 00	0.043 10	0.350 00	0.045 00	0.046 50
	$4E_{sa,a}^{(011)}$	0.058 00	0.040 00	0.050 00	0.050 84	0.052 20	0.053 90
$V_{s^*a,xa}$	$4E_{s^*a,xa}^{(110)}$	0.020 00	0.020 00	0.017 24	0.020 00	0.018 00	0.018 60
	$4E_{s^*a,xa}^{(011)}$	0.040 00	0.100 00	0.034 48	0.063 88	0.036 00	0.037 20
$V_{xa,xa}$	$4E_{xa,xa}^{(110)}$	0.320 00	0.376 90	0.275 90	0.432 32	0.288 00	0.298 00
$U_{xa,xa}$	$4E_{xa,xa}^{(011)}$	-0.050 00	-0.200 00	-0.043 10	-0.277 10	-0.045 00	-0.046 50
	$4E_{xa,ya}^{(110)}$	1.240 00	0.660 00	1.069 00	1.009 16	0.510 00	1.153 00
	$4E_{xa,ya}^{(011)}$	-1.000 00	-1.200 00	-0.862 10	-1.079 60	-0.900 00	-0.930 00
$V_{sc,sc}$	$4E_{sc,sc}^{(110)}$	-0.020 00	-0.010 00	-0.032 24	-0.016 02	-0.018 00	-0.018 60
$V_{sc,xc}$	$4E_{sc,xc}^{(110)}$	0.072 00	0.073 00	0.062 07	0.370 00	0.064 80	0.067 00
	$4E_{sc,xc}^{(011)}$	0.020 00	0.040 00	0.017 24	0.027 96	0.018 00	0.018 60
$V_{s^*c,xc}$	$4E_{s^*c,xc}^{(110)}$	0.010 00	0.030 00	0.008 62	0.420 00	0.009 00	0.009 30
	$4E_{s^*c,xc}^{(011)}$	0.093 50	0.030 00	0.080 61	0.068 23	0.084 15	0.087 00
$V_{xc,xc}$	$4E_{xc,xc}^{(110)}$	0.280 00	0.495 35	0.215 50	0.365 71	0.252 00	0.260 00
$U_{xc,xc}$	$4E_{xc,xc}^{(011)}$	-0.100 00	-0.166 95	-0.086 21	-0.126 64	-0.090 00	-0.093 00
	$4E_{xc,yc}^{(110)}$	0.600 00	0.870 00	0.945 00	0.448 80	0.140 00	0.456 35
	$4E_{xc,yc}^{(011)}$	-1.300 00	-2.200 00	-1.120 70	-1.459 20	-1.170 00	-1.000 00
	λ_a	0.140 00	0.140 00	0.324 33	0.324 33	0.140 00	0.022 33
	λ_c	0.058 00	0.008 00	0.058 00	0.008 00	0.131 00	0.130 67

$$E_{\pm} \equiv \bar{E} \pm \Delta, \quad \bar{E} \equiv \frac{E_a + E_c}{2},$$

$$\nu_a^+ = \frac{\Delta + E_{\Delta}}{\sqrt{2}\sqrt{\Delta^2 + \Delta E_{\Delta}}} = \nu_c^-, \quad \nu_c^+ = \frac{V}{\sqrt{2}\sqrt{\Delta^2 + \Delta E_{\Delta}}} = -\nu_a^- \quad (3)$$

$$E_{\Delta} \equiv \frac{E_a - E_c}{2}, \quad \Delta \equiv \sqrt{E_{\Delta}^2 + V^2}, \quad (1)$$

$$|n \pm\rangle = \nu_a^{\pm} |na\rangle + \nu_c^{\pm} |nc\rangle, \quad (2)$$

In Eq. (3) n refers to the basis function for electrons (s) or holes (l , h , or so) defined in Eqs. (1)–(3) of Ref. 6.

Using Eqs. (1)–(3) above along with the quantities in Table II we calculate the inverse effective masses (m_0/m_{zz}^*) at Γ .⁸ A little algebra yields all four masses, with subscripts

e , lh , hh , and soh denoting the electron, and the light, heavy, and split-off holes, respectively. In Eqs. (4)–(7) m_0 is the free-electron mass and a is the conventional unit-cell cube edge:

$$\begin{aligned} \frac{m_0}{m_e^*} = \frac{2m_0}{\hbar^2} \left(\frac{a}{4} \right)^2 & \left\{ -\sigma_a^+ \sigma_c^+ V_{s,s} - 4[(\sigma_a^+)^2 V_{sa,sa} + (\sigma_c^+)^2 V_{sc,sc}] \right. \\ & + \frac{2}{3} \frac{[4(\sigma_c^+ \varrho_a^{l,+} V_{sc,xc} - \sigma_a^+ \varrho_c^{l,+} V_{sa,xa}) + (\sigma_a^+ \varrho_c^{l,+} V_{sa,pc} - \sigma_c^+ \varrho_a^{l,+} V_{pa,sc})]^2}{E_+^{(e)} - E_-^{(lh)}} \\ & + \frac{1}{3} \frac{[4(\sigma_c^+ \varrho_a^{so,+} V_{sc,xc} - \sigma_a^+ \varrho_c^{so,+} V_{sa,xa}) + (\sigma_a^+ \varrho_c^{so,+} V_{sa,pc} - \sigma_c^+ \varrho_a^{so,+} V_{pa,sc})]^2}{E_+^{(e)} - E_-^{(soh)}} \\ & + \frac{2}{3} \frac{[4(\sigma_c^+ \varrho_c^{l,+} V_{sc,xc} + \sigma_a^+ \varrho_a^{l,+} V_{sa,xa}) + (\sigma_a^+ \varrho_c^{l,+} V_{sa,pc} + \sigma_c^+ \varrho_a^{l,+} V_{pa,sc})]^2}{E_+^{(e)} - E_+^{(lh)}} \\ & \left. + \frac{1}{3} \frac{[4(\sigma_c^+ \varrho_c^{so,+} V_{sc,xc} + \sigma_a^+ \varrho_a^{so,+} V_{sa,xa}) + (\sigma_a^+ \varrho_c^{so,+} V_{sa,pc} + \sigma_c^+ \varrho_a^{so,+} V_{pa,sc})]^2}{E_+^{(e)} - E_+^{(soh)}} \right\}, \end{aligned} \quad (4)$$

$$\begin{aligned} \frac{m_0}{m_{lh}^*} = \frac{2m_0}{\hbar^2} \left(\frac{a}{4} \right)^2 & \left\{ \varrho_a^{l,+} \varrho_c^{l,+} V_{x,y} - \frac{2}{3} [(\varrho_c^{l,+})^2 (5V_{xa,xa} + U_{xa,xa}) + (\varrho_a^{l,+})^2 (5V_{xc,xc} + U_{xc,xc})] \right. \\ & + \frac{2}{3} \frac{[4(\sigma_a^+ \varrho_a^{l,+} V_{sc,xc} + \sigma_c^+ \varrho_c^{l,+} V_{sa,xa}) - (\sigma_c^+ \varrho_a^{l,+} V_{sa,pc} + \sigma_a^+ \varrho_c^{l,+} V_{pa,sc})]^2}{E_-^{(lh)} - E_-^{(e)}} \\ & + \frac{2}{3} \frac{[4(\sigma_c^+ \varrho_a^{l,+} V_{sc,xc} - \sigma_a^+ \varrho_c^{l,+} V_{sa,xa}) + (\sigma_a^+ \varrho_c^{l,+} V_{sa,pc} - \sigma_c^+ \varrho_a^{l,+} V_{pa,sc})]^2}{E_-^{(lh)} - E_+^{(e)}} + \frac{2}{3} \frac{(4\varrho_c^{l,+} V_{s^*a,xa} - \varrho_a^{l,+} V_{s^*a,pc})^2}{E_-^{(lh)} - E_{s^*a}} \\ & \left. + \frac{2}{3} \frac{(4\varrho_a^{l,+} V_{s^*c,xc} - \varrho_c^{l,+} V_{pa,s^*c})^2}{E_-^{(lh)} - E_{s^*c}} + \frac{1}{3} \frac{V_{x,y}^2}{E_-^{(lh)} - E_+^{(lh)}} \right\}, \end{aligned} \quad (5)$$

$$\begin{aligned} \frac{m_0}{m_{hh}^*} = \frac{2m_0}{\hbar^2} \left(\frac{a}{4} \right)^2 & \left\{ \varrho_a^{l,+} \varrho_c^{l,+} V_{x,x} - 2[(\varrho_c^{l,+})^2 (V_{xa,xa} + U_{xa,xa}) + (\varrho_a^{l,+})^2 (V_{xc,xc} + U_{xc,xc})] + \frac{1}{3} \frac{V_{x,y}^2}{E_-^{(lh)} - E_+^{(e)}} \right. \\ & \left. + \frac{2}{3} V_{x,y}^2 \frac{[\varrho_a^{so,+} \varrho_c^{l,+} + \varrho_c^{so,+} \varrho_a^{l,+}]^2}{E_-^{(lh)} - E_+^{(soh)}} + \frac{2}{3} V_{x,y}^2 \frac{[\varrho_a^{so,+} \varrho_c^{l,+} - \varrho_c^{so,+} \varrho_a^{l,+}]^2}{E_-^{(lh)} - E_-^{(soh)}} \right\}, \end{aligned} \quad (6)$$

$$\begin{aligned} \frac{m_0}{m_{soh}^*} = \frac{2m_0}{\hbar^2} \left(\frac{a}{4} \right)^2 & \left\{ \varrho_a^{so,+} \varrho_c^{so,+} V_{x,x} - \frac{4}{3} [(\varrho_c^{so,+})^2 (2V_{xa,xa} + U_{xa,xa}) + (\varrho_a^{so,+})^2 (2V_{xc,xc} + U_{xc,xc})] \right. \\ & + \frac{1}{3} \frac{[4(\sigma_c^+ \varrho_a^{so,+} V_{sc,xc} - \sigma_a^+ \varrho_c^{so,+} V_{sa,xa}) + (\sigma_a^+ \varrho_c^{so,+} V_{sa,pc} - \sigma_c^+ \varrho_a^{so,+} V_{pa,sc})]^2}{E_-^{(soh)} - E_+^{(e)}} \\ & + \frac{1}{3} \frac{[4(\sigma_a^+ \varrho_a^{so,+} V_{sc,xc} + \sigma_c^+ \varrho_c^{so,+} V_{sa,xa}) - (\sigma_a^+ \varrho_c^{so,+} V_{pa,sc} + \sigma_c^+ \varrho_a^{so,+} V_{sa,pc})]^2}{E_-^{(soh)} - E_-^{(e)}} + \frac{2}{3} V_{x,y}^2 \frac{[\varrho_a^{so,+} \varrho_c^{l,+} - \varrho_c^{so,+} \varrho_a^{l,+}]^2}{E_-^{(soh)} - E_-^{(lh)}} \\ & \left. + \frac{2}{3} V_{x,y}^2 \frac{[\varrho_a^{so,+} \varrho_c^{l,+} + \varrho_c^{so,+} \varrho_a^{l,+}]^2}{E_-^{(soh)} - E_+^{(e)}} + \frac{1}{3} \frac{(4\varrho_c^{so,+} V_{s^*a,xa} - \varrho_a^{so,+} V_{s^*a,pc})^2}{E_-^{(soh)} - E_{s^*a}} + \frac{1}{3} \frac{(4\varrho_a^{so,+} V_{s^*c,xc} - \varrho_c^{so,+} V_{pa,s^*c})^2}{E_-^{(soh)} - E_{s^*c}} \right\}. \end{aligned} \quad (7)$$

TABLE II. Energies and coefficients for the bands in terms of the generic notation of Eqs. (1)–(3). The “+” solutions correspond to conduction bands, the “−” solutions to valence bands. The names “electron” and “hole” refer to both solutions: for example, “ $e+$ ” denotes the lowest conduction band, while “ $lh-$ ” denotes the light-hole valence band. The subscript μ refers to anions (a) or cations (c). In the table below we define $E_{s\mu}^{\text{eff}} \equiv E_{s\mu} + 3V_{s\mu,s\mu}$, $E_{p\mu}^{\text{eff}} \equiv E_{p\mu} + 2V_{x\mu,x\mu} + U_{x\mu,x\mu}$.

Quantity in Eqs. (1)–(3)	Electrons	Light holes	Heavy holes	Split-off holes
E_{μ}	$E_{s\mu}^{\text{eff}}$	$E_{p\mu}^{\text{eff}} + \lambda_{\mu}$	$E_{p\mu}^{\text{eff}} + \lambda_{\mu}$	$E_{p\mu}^{\text{eff}} - 2\lambda_{\mu}$
V	$V_{s,s}$	$V_{x,x}$	$V_{x,x}$	$V_{x,x}$
E_{\pm}	$E_{\pm}^{(e)}$	$E_{\pm}^{(lh)}$	$E_{\pm}^{(lh)}$	$E_{\pm}^{(soh)}$
ν_{μ}^{+}	σ_{μ}^{+}	$\varrho_{\mu}^{l,+}$	$\varrho_{\mu}^{l,+}$	$\varrho_{\mu}^{so,+}$
Δ	$\Delta^{(e)}$	$\Delta^{(lh)}$	$\Delta^{(lh)}$	$\Delta^{(soh)}$

With expressions (4)–(7) we proceed to fit the bands of GaAs, AlAs, GaSb, AlSb, InAs, and InP at $T=300$ K; separately examining the components of each inverse mass expression clarifies which couplings and second-order corrections are of greatest importance. We determined the parameters manually, employing in addition to the foregoing formulas a computer program that calculates the first-order change in any selected band energy and mass at an arbitrary point \mathbf{k} under a change to each of the parameters (the others being held fixed). Several of the parameter sets here were determined using nearest-neighbor sp^3s^* sets as the starting points. In this procedure, the second-nearest-neighbor parameters are slowly “turned on,” and we found this approach to be successful in most cases. By contrast, beginning with a second-nearest-neighbor sp^3 set and then turning on the s^* couplings proved much less successful. This behavior is doubtless due to the fact that the nearest-neighbor s^* interactions are often large, in contrast to the second-nearest-neighbor interactions, which are usually smaller.

The results of the foregoing procedure are displayed in Figs. 1–6 and the parameters are listed in Table I. In Table

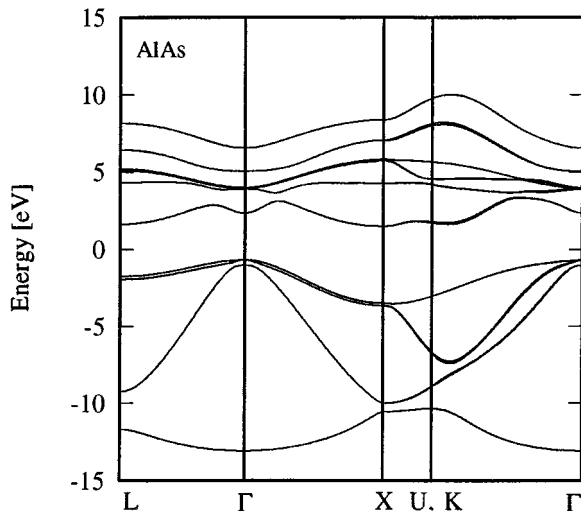


FIG. 1. Bands of AlAs as reproduced by the parameters of Table I.

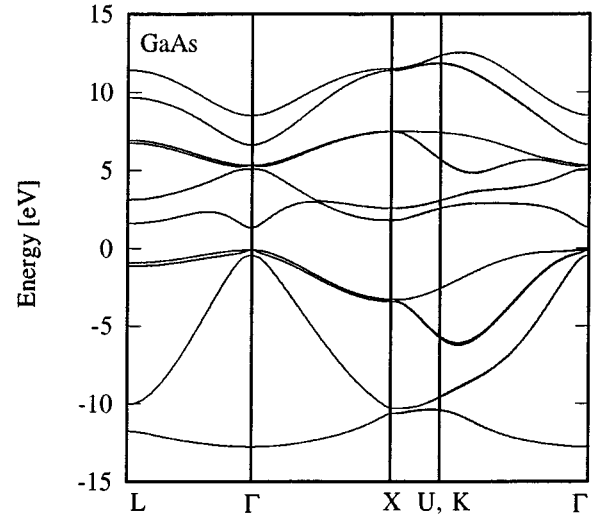


FIG. 2. Bands of GaAs as reproduced by the parameters of Table I.

III we give the effective masses and energy gaps reproduced by the parameters of Table I; we tailor the bands to fit the quantities of greatest importance in typical heterostructure calculations for devices grown on [001]-oriented substrates. For InAs and InP we fit the conduction-band intervalley separations $E_{X\Gamma}$ and $E_{L\Gamma}$ to their low-temperature values since we could not find room-temperature data. Note that we adopt a more flexible approach than do Loehr and Talwar,⁵ who rigidly fix the electron and heavy-hole masses along with certain of the gaps. That is, we compromise slightly on some of the other gaps and masses in order to achieve good fits for the light-hole and X-valley masses. The extra freedom afforded by the second-nearest-neighbor parameters, together with the analytic results, yields much better fits for the AlAs electron and light-hole masses than was the case with the spin-orbit nearest-neighbor model;⁶ we have even improved the fits over our previous second-nearest-neighbor effort.⁴ Finally, since these parameters are intended

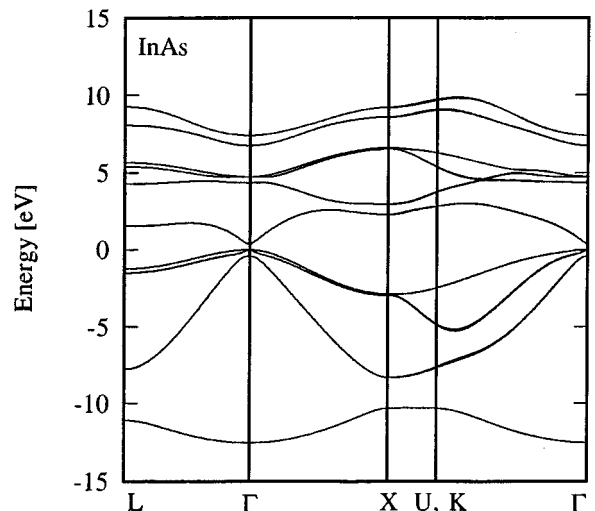


FIG. 3. Bands of InAs as reproduced by the parameters of Table I.

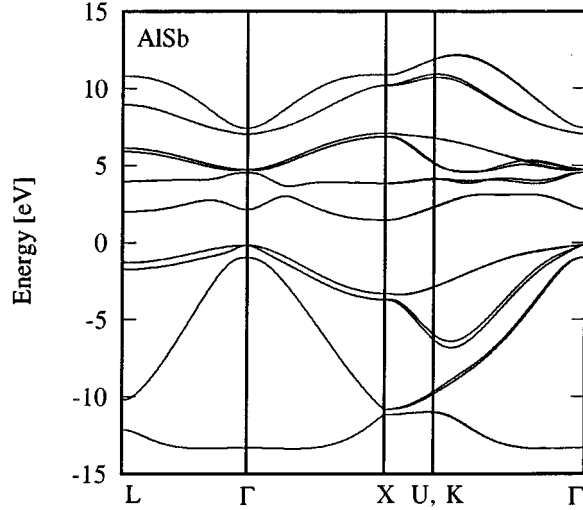


FIG. 4. Bands of AlSb as reproduced by the parameters of Table I.

for use with [001]-oriented heterostructures we choose to emphasize Γ - and X -valley features, occasionally at the expense of the L valleys: as a result, the gaps and masses associated with the former are generally well reproduced.

The sole remarkable exception to this trend is InP, which has a large electron–light-hole effective-mass mismatch⁹ $|m_{lh}^*/m_e^*| = 0.12/0.079 = 1.52$; our parametrization yields a mismatch of only 1.15. While we did find parametrizations giving a somewhat greater mismatch, this improvement came only at the considerable expense of other band-structure features, most notably the heavy-hole mass. This difficulty in fitting both the electron and light-hole masses of InP suggests that we may have discovered a limitation of the second-nearest-neighbor sp^3s^* model instead of a mere failure to find the best parametrization.

Examining Eqs. (4) and (5) we see that this difficulty is no accident, for under a few physically reasonable and minimally restrictive assumptions ($V_{s,s}$ large and negative, nearest-neighbor parameters of greater magnitude than second-nearest-neighbor parameters) the equations show that

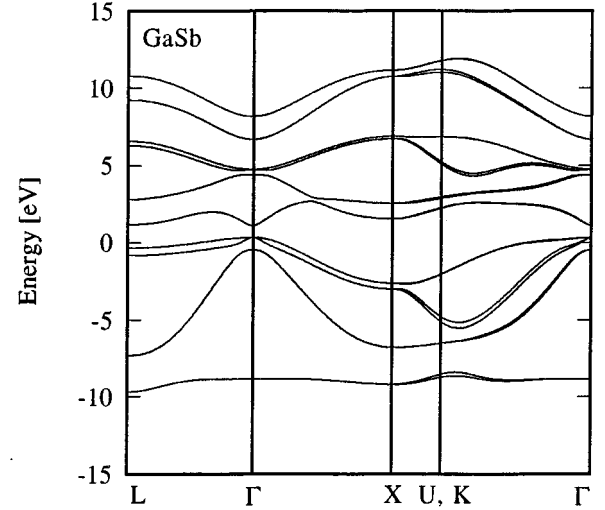


FIG. 5. Bands of GaSb as reproduced by the parameters of Table I.

there is an upper limit on the achievable electron–light-hole effective-mass mismatch. To simplify the discussion, we denote the electron–light-hole coupling term in Eq. (4) by $\frac{2}{3}\mu$. Under the assumptions above, we see that the electron–split-off hole term of Eq. (4) is approximately (or perhaps less than) half this value, $\frac{1}{3}\mu$, and that the second term is small. The remaining terms of Eq. (4) are negative—the first (the nearest-neighbor contribution to the d^2H/dk^2 term) is often sizable—so that we have $|m_0/m_e^*| \lesssim \mu$. In contrast, the electron–light-hole coupling, though largest, is only one of at least four negative contributors to Eq. (5): the others couple the light hole to the “heavy” conduction band, s^*a bands, and s^*c bands. The positive terms of Eq. (5) usually cannot cancel these three negative terms since $V_{x,x}$ is often small and the s -like valence band is generally lowest and quite remote. Hence it follows that $|m_0/m_{lh}^*| \gtrsim \frac{2}{3}\mu$, yielding an upper limit $|m_{lh}^*/m_e^*| \lesssim \frac{3}{2}$. Since the InP mismatch lies at this limit it follows that whenever reproducing both the electron and light-hole masses to high accuracy is desirable a more complete model is probably needed.

TABLE III. Energy gaps and effective masses reproduced by the tight-binding parameters of Table I. Energies are expressed in eV, masses in terms of the free electron mass. $E_{X\Gamma}$ and $E_{L\Gamma}$ are the differences in energy between the conduction-band X - and L -valley minima and the Γ -valley minimum, respectively, and m_e^* is the conduction-band mass at Γ .

Theory	GaAs	AlAs	GaSb	AlSb	InAs	InP
$E_g(\Gamma)$	1.424	3.022	0.754	2.300	0.354	1.342
$E_{X\Gamma}$	0.482	-0.856	0.443	-0.684	1.917	0.894
$E_{L\Gamma}$	0.313	-0.693	0.076	-0.125	1.166	0.611
Δ_0	0.366	0.338	0.800	0.785	0.415	0.141
m_e^*	0.068	0.16	0.048	0.13	0.025	0.091
$m_{X,l}^*$	1.32	1.34	1.30	1.67	1.30	1.26
$m_{X,t}^*$	0.31	0.26	0.33	0.28	0.27	0.34
$m_{L,l}^*$	1.39	1.14	1.13	1.82	2.11	1.64
$m_{L,t}^*$	0.13	0.15	0.098	0.20	0.12	0.13
m_{lh}^*	0.071	0.15	0.050	0.11	0.028	0.10
m_{hh}^*	0.41	0.48	0.36	0.34	0.39	0.44
m_{soh}^*	0.14	0.25	0.15	0.20	0.10	0.18

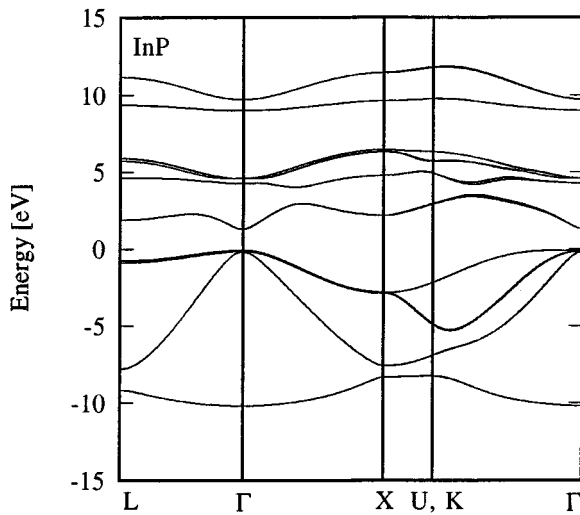


FIG. 6. Bands of InP as reproduced by the parameters of Table I.

In light of the foregoing discussion, it is instructive to consider the role played by the gap in determining the maximum possible reproducible light-hole–electron mass ratio. From the expressions above, we see that the maximum positive contribution to the electron inverse mass occurs in the limit of small spin-orbit coupling, and that in this case both the electron–light-hole and electron–split-off hole terms scale as $1/E_g$. The above analysis also makes it clear that for reasonable parameters the remaining terms of the electron

expression tend to reduce the electron inverse mass; hence the maximum achievable inverse electron mass will be μ and will scale as $1/E_g$. Similarly, we have seen that reasonable parameters result in an inverse light-hole mass with minimum magnitude $\frac{2}{3}\mu$. Since this term also scales as $1/E_g$, we see that the maximum ratio $|m_{lh}^*/m_e^*| \approx \frac{3}{2}$, independent of the gap. Finally, we remark that as these parameters that are fit to bulk band structures will be employed in heterostructure calculations *all* materials effects we wish to model must be included via the parameters. Hence the reproducible gaps and masses are intimately and inextricably connected to the tight-binding parameters.

In conclusion, we have derived analytic formulas for the electron and light, heavy, and split-off hole masses at Γ in the spin-orbit, second-nearest-neighbor sp^3s^* model. We have discussed the utility of these results in terms of both choosing and parametrizing a model for use in heterostructure calculations. We have employed these formulas in fitting the bands of six common III-V materials (GaAs, AlAs, GaSb, AlSb, InAs, and InP), achieving generally good fits of all masses and gaps important in [001]-oriented heterostructure calculations. Moreover, using the formulas derived here we have demonstrated that the second-nearest-neighbor sp^3s^* model can reproduce a light-hole–electron effective-mass ratio of at most 1.5. Hence we conclude that the difficulty encountered in fitting both the electron and light-hole masses of InP is due to an *intrinsic* characteristic, and *not* a failure to find its best parametrization.

We gratefully acknowledge the support of Texas Instruments, Inc.

¹P. Vogl, Harold P. Hjalmarson, and John D. Dow, *J. Phys. Chem. Solids* **44**, 365 (1983).

²Timothy B. Boykin, Jan P. A. van der Wagt, and James S. Harris, Jr., *Phys. Rev. B* **43**, 4777 (1991).

³D. N. Talwar and C. S. Ting, *Phys. Rev. B* **25**, 2660 (1982).

⁴Timothy B. Boykin, *Phys. Rev. B* **54**, 8107 (1996).

⁵J. P. Loehr and D. N. Talwar, *Phys. Rev. B* **55**, 4353 (1997).

⁶Timothy B. Boykin, Gerhard Klimeck, R. Chris Bowen, and Roger Lake, *Phys. Rev. B* **56**, 4102 (1997).

⁷J. C. Slater and G. F. Koster, *Phys. Rev.* **94**, 1498 (1954).

⁸Timothy B. Boykin, *Phys. Rev. B* **52**, 16 317 (1995).

⁹The compound semiconductor InP is treated exhaustively in Sadao Adachi, *Physical Properties of III-V Semiconductor Compounds: InP, InAs, GaAs, GaP, InGaAs, and InGaAsP* (Wiley, New York, 1992); the electron and light-hole masses are discussed in detail on pp. 90–93. Experiments cited therein give the electron mass in the range $0.077\text{--}0.080m_0$ and the light-hole mass as $0.12 \pm 0.01m_0$. Thus even the smallest experimentally supported ratio $|m_{lh}^*/m_e^*| = 0.11/0.08 = 1.375$, which is rather difficult to reproduce with reasonable parameters.